



# Isotopic evidence for rapid continental growth in an extensional accretionary orogen: The Tasmanides, eastern Australia

A.I.S. Kemp<sup>a,\*</sup>, C.J. Hawkesworth<sup>b</sup>, W.J. Collins<sup>a</sup>, C.M. Gray<sup>a</sup>, P.L. Blevin<sup>c</sup>, EIMF<sup>d</sup>

<sup>a</sup> School of Earth and Environmental Science, James Cook University, Townsville, Australia

<sup>b</sup> Department of Earth Sciences, University of Bristol, Bristol, UK

<sup>c</sup> NSW Department of Primary Industries, PO Box 344, NSW, Australia

<sup>d</sup> Edinburgh Ion Microprobe Facility, University of Edinburgh, Edinburgh, UK

## ARTICLE INFO

### Article history:

Received 10 November 2008

Received in revised form 1 May 2009

Accepted 8 May 2009

Available online 16 June 2009

Editor: R.W. Carlson

### Keywords:

continental growth

Nd isotopes

Hf isotopes

tectonics

Tasmanides

granite

## ABSTRACT

The trace element signature of Earth's continental crust resembles that of arc lavas, but the continents may have formed during ancient igneous pulses that are hard to reconcile with supra-subduction zone magmatism. We explore the role of coupled arc–back-arc accretionary processes in crust generation by considering the tectonic context of whole rock Nd isotope and zircon Hf–O isotope data from igneous rocks of the Australian Tasmanides (515–230 Ma), which is thought to have evolved by the repeated opening and closure of sediment-filled back-arc basins behind a long-lived subduction zone. The significance of this process for continental crust formation has yet to be evaluated from an isotopic perspective. Granitic rocks in this area define striking secular  $\varepsilon_{\text{Nd}}-\varepsilon_{\text{Hf}}-\delta^{18}\text{O}$  trends that correlate with the pattern of deformational events and register changes in magma source during tectonic activity. These trends reveal that juvenile magmatic input was enhanced during extensional, back-arc rifting episodes that immediately followed crustal thickening, suggesting a relationship between slab rollback and continental growth. Interaction between juvenile magma and sedimentary units deposited during a preceding back-arc rifting cycle was integral to the formation of stable continental material. This highlights the importance of back-arc environments for both the generation and differentiation of continental crust. The juvenile component within the Tasmanide igneous rocks increased from the Cambrian to the Triassic, consistent with a diminished input from craton-derived metasedimentary material as the subduction zone migrated outboard of the Gondwana margin. Subduction zone retreat formed large tracts of new crust in eastern Australia at comparable rates to crust generation at modern island arcs, providing a mechanism for rapid continental growth at convergent margins. Using isotopic tracers to link tectonic evolution and crust generation in modern and ancient orogens can lead to a better understanding of the geodynamic controls on planetary differentiation.

© 2009 Elsevier B.V. All rights reserved.

## 1. A continental paradox

Ascertaining the geodynamic controls on continental crust formation holds the key to understanding the differentiation of the silicate Earth. Yet, a paradox has emerged concerning the processes of continent generation (here defined as the addition of mantle-derived material to the continental crust). On the one hand, it is well established that the composition of the continental crust broadly resembles that of intermediate, subduction-related volcanic rocks, underpinning the popular view that arc magmatism is the prevalent mode of continent generation (Taylor, 1967; Davidson and Arculus, 2006). However, radiogenic isotope evidence (e.g. Stein and Hofmann, 1994; McCulloch and Bennett, 1994; Condie, 1998; Kemp et al., 2006) suggests that much of the extant continental mass formed during short (100–300 Ma)

bursts of juvenile magmatism of near-global extent, notably around 1.9, 2.7 and 3.3–3.5 Ga. The isotopic legacy of ancient, pulsed crust extraction has also recently been inferred in the complementary mantle residues (Parman, 2007; Pearson et al., 2007). Whether arc magmatism can engender peaks of accelerated continental crust generation on a global scale is questionable, particularly as there are no pronounced peaks within the last billion years when a plate tectonic regime prevailed on Earth (Condie, 1998). Episodic crustal growth has instead been attributed to mantle plumes (Stein and Hofmann, 1994; Condie, 1998), implying that continent formation reflects deep-seated thermal anomalies rather than interactions between lithospheric plates.

What then is the role of subduction processes like those operating at the present day in continental evolution? Is the 'subduction factory' one of crustal recycling and differentiation rather than growth (Plank, 2005)? Models for continent formation at Phanerozoic convergent plate boundaries envisage both vertical accretion, via under- or intra-plating of arc magmas from the mantle wedge (e.g. Davidson and Arculus, 2006), as well as the lateral accretion of juvenile oceanic arcs

\* Corresponding author. Tel.: +61 74781 5052.

E-mail address: [tony.kemp@jcu.edu.au](mailto:tony.kemp@jcu.edu.au) (A.I.S. Kemp).

or oceanic plateaus (e.g. North America: Samson et al., 1989; Patchett and Chase, 2002; Irish Caledonides, Draut and Cliff, 2001), or subduction–accretion complexes (e.g. central Asia: Sengor et al., 1993). These crustal growth models emphasise accretionary processes at the arc front. Yet, continental material formed in this way is prone to destruction by sediment subduction or subduction erosion (Clift and Vannuchi, 2004), and/or density foundering (Zandt et al., 2004).

A contrasting, but comparatively neglected, crust generation mechanism in subduction settings involves the opening of back-arc basins during slab rollback, as has dominated the recent evolution of the western Pacific arc systems, with accretion of juvenile material during subsequent compression and back-arc closure. This process is ascribed a key role in the development of vast Paleozoic–Mesozoic orogens along the Paleo-Pacific Gondwana margin (e.g., Collins 2002a; Cawood, 2005). However, using bulk rock isotopes to quantify juvenile continental additions in these orogens, such as in the Tasmanides of eastern Australia, is hampered by extensive reworking of old crust (McCulloch and Chappell, 1982; Jahn et al., 2000). This imparts low initial  $^{143}\text{Nd}/^{144}\text{Nd}$  ratios in granites and obscures the volume and composition of contemporary mantle input.

Here, we explore the significance of coupled arc and back-arc processes for continental crust generation with reference to the Tasmanides and by combining whole rock Nd isotope data with the distinctive archive of oxygen and hafnium isotopes in granite-hosted zircon. Zircon-hosted isotope tracer information has potential for distinguishing juvenile contributions to felsic igneous suites (Griffin et al., 2002; Lackey et al., 2005; Kemp et al., 2007; Yang et al., 2007; Bolhar et al., 2008), and thus for monitoring crustal addition during magmatic episodes. Our goal is to use isotope data from the Tasmanide

igneous rocks to (1) deduce the timing and site of crust generation, and link this to tectonic activity during the evolution of the orogen, and (2) assess the wider importance of subduction zone retreat for continental crust formation.

## 2. Geological and tectonic framework of the Tasmanides

From west to east, the Tasmanides comprise the Delamerian (~515–490 Ma), Lachlan (485–340 Ma) and New England orogens (305–230 Ma) (Fig. 1). This orogenic ensemble occupies the eastern third of Australia and formed successively and progressively outboard of the Pacific-facing rim of the newly assembled Gondwana Supercontinent (see reviews by Gray and Foster, 2004, Glen, 2005 and Cawood and Buchan, 2007). Each Tasmanide terrane is dominated by granitic batholiths and Paleozoic metasedimentary rocks, the latter being craton-derived turbidites for the Delamerian and Lachlan orogens, and accretionary prism materials for the arc-proximal New England orogen. Unambiguous crystalline Precambrian basement is limited to the westernmost Delamerian orogen. The Tasmanide sedimentary units were regionally metamorphosed to lower greenschist facies, locally reaching upper amphibolite facies, and overprinted by a number of short (<10–15 Ma) but intense compressional deformations. Thin belts of mafic-intermediate metavolcanic rock, with subordinate ultramafic components, are exposed along major faults. These ‘greenstone’ belts, which form the oceanic substrate to the turbidites (Fergusson, 2003), become younger to the east and have subduction-related geochemical affinity (e.g. Crawford and Keays, 1987).

Granitic rocks of the Tasmanides include the archetypal strongly peraluminous ‘S-types,’ metaluminous ‘I-types’ and the petrologically

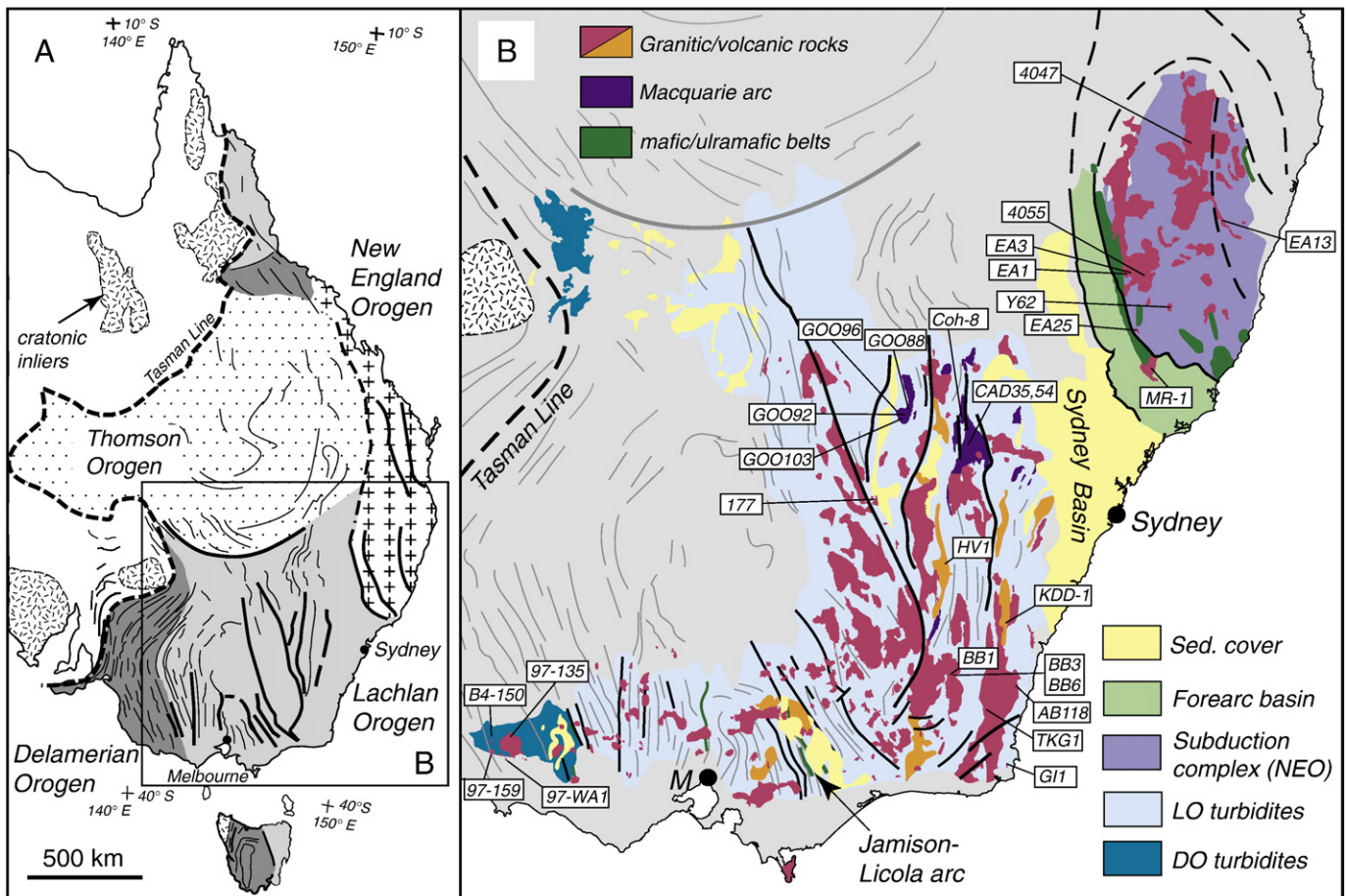


Fig. 1. Simplified geological maps of the Tasmanides (modified after Gray and Foster, 2004), showing the location of the sampled units (in boxes) for which zircon isotope data are reported (DO, Delamerian Orogen; LO, Lachlan Orogen; M, Melbourne; NEO, New England Orogen).

distinctive ‘A-types.’ S-type granites tend to be the oldest in a given area, whereas A-type emplacement commonly post-dates compressional deformation and is associated with extensional structures. The I–S-type paradigm demands contrasting meta-igneous and metasedimentary source rocks for these granites (White and Chappell, 1977). However, I- and S-type granites from each Tasmanide terrane define a Sr–Nd isotope continuum bracketed between a mantle-like component and the host metasedimentary package (Fig. 2), attesting to the importance of mixing processes in their genesis (Gray, 1984; Collins, 1998; Foden et al. 2002). Isotope systematics of the A-type granites broadly conform to this mixing array (Fig. 2) but are complicated by Sr isotope disturbance during hydrothermal alteration (Wormald et al.,

2004). Nevertheless, Hf isotope in zircon variations reveal that interaction between juvenile material and older crust was also integral to the evolution of A-type magmas (Kemp et al., 2005). Given the isotopic evidence for mixed sources for the Tasmanide granites, the I- and S-type notation is used below in a non-genetic sense to convey the general metaluminous versus strongly peraluminous character of granitic suites.

Recent tectonic models attribute the development of the Tasmanides to alternating compressive and extensional dynamics associated with a west-dipping subduction zone that migrated oceanward from near the cratonic Gondwana margin in the Cambrian to the easternmost part of the current Australian mainland by the Permian, and ultimately to the New Zealand–Tonga–Kermadec arc at the present day (Foster and Gray, 2000; Collins 2002a,b; Gray and Foster, 2004; Glen 2005; Cawood, 2005; Foster et al., 2005). The Tasmanides are therefore viewed in terms of accretionary, rather than collisional, processes. Collins and Richards (2008) have sought to link the geological elements of the Delamerian, Lachlan and New England orogens in terms of ‘tripartite associations,’ which consist of (1) belts of S-type granite and associated high T–low P metamorphic complexes, (2) outboard oceanic arc sequences, remnants of which are preserved as the greenstones, and (3) intervening and slightly younger sediment-filled back-arc basins, into which I-type plutons are emplaced. Four such tripartite associations are recognised, of Middle Cambrian, Cambrian–Ordovician, Silurian and Carboniferous age. Each of these is regarded as a distinct phase of arc retreat, magmatism, and back-arc rifting that followed a major compressive event associated with the closure of a precursor back-arc basin (Collins and Richards, 2008). The tripartite concept establishes geodynamic linkages between the three Tasmanide terranes and has implications for crust generation processes that can be explored using isotope systematics of igneous rocks.

### 3. Samples and analytical methods

To obtain an isotopic overview of Tasmanide magmatism we present new whole rock and zircon-derived isotope data from key igneous units of various ages, and combine this with previously published data. The new data are from igneous rocks of the eastern Delamerian Orogen, the eastern Lachlan Orogen, and the southern lobe of the New England Orogen (Fig. 1). These correspond to the Cambrian–Ordovician, Silurian and Carboniferous tripartite associations, respectively, of Collins and Richards (2008). The Delamerian samples straddle a major Trans-Gondwanan contractional event, the Ross–Delamerian orogeny (which commenced by ~514 Ma, Foden et al., 2006), and include pre- to syn-compressional hornblende tonalites, late syn-compressional peraluminous granodiorites, and post-compressional A-type granites. The Lachlan samples range from intrusives of the Macquarie arc (484–439 Ma), representing an early intra-oceanic stage of the orogen, through to S-type, I-type and A-type plutons that post-date the contractional Benambran orogeny (440–430 Ma). S-type and younger I-type intrusives of the New England Orogen span a major rifting event, involving formation of the Sydney–Bowen basin (270–280 Ma), and the compressional deformation of the Hunter–Bowen orogeny (~265–250 Ma; Cawood and Buchan, 2007).

The whole rock Sm–Nd isotope data (Table 1) was acquired at La Trobe University, Melbourne, using a Finnegan MAT 262 solid-source mass spectrometer (see Huang et al., 2003). Techniques for the in situ isotope analysis of zircon are detailed elsewhere (Kemp et al., 2006, 2007; supplementary data). In brief, zircon grains were encapsulated in epoxy resin, polished to expose their interior, and dated by ion microprobe (U–Th)–Pb isotope analysis. The oxygen isotope compositions (Table 2) were measured with a Cameca ims 1270, using a primary  $^{133}\text{Cs}^+$  beam and charge compensation by normal incidence electron gun. Sample zircon data were normalised to bracketing analyses of zircon 91500 ( $\delta^{18}\text{O}$  10.07 ± 0.03‰ VSMOW, Valley, 2003) to correct for instrumental mass fractionation. Hafnium isotope analysis

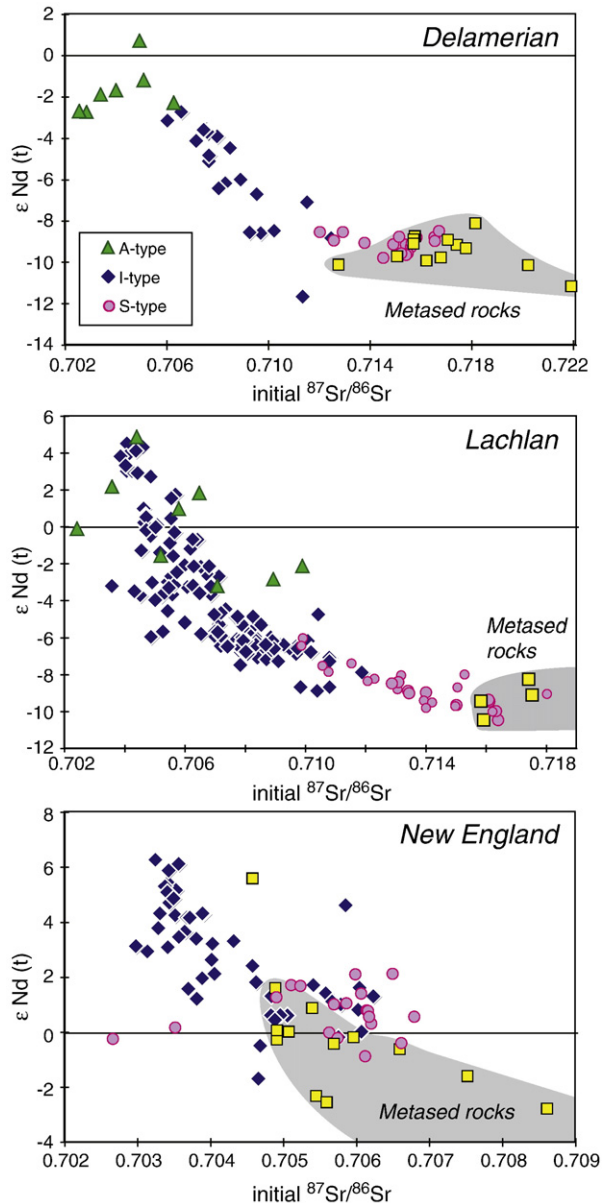


**Fig. 2.** Plots of  $\epsilon_{\text{Nd}}$  versus initial  $^{87}\text{Sr}/^{86}\text{Sr}$  for igneous rocks of the Delamerian, Lachlan and New England orogens, compared to basement metasedimentary rocks in each area (squares, calculated at 500 Ma, 430 Ma and 300 Ma, respectively). Data are from this study and compiled from published sources as follows. Delamerian Orogen: Turner et al. (1993). Lachlan Orogen: McCulloch and Chappell (1982), Chappell et al. (1991), Maas et al. (1997), King et al. (1997), Keay et al. (1997), Collins et al. (2006), and Crawford et al. (2007). New England Orogen: Hensel et al. (1985), and Bryant et al. (1997). The data in Hensel et al. (1985) were recalculated according to the emplacement ages quoted by Landenberger et al. (1995) and Bryant et al. (1997). Note that Sr–Nd isotope data for A-type granites of the New England Orogen are as yet unavailable.

**Table 1**  
Bulk rock Sm–Nd isotope data for igneous rocks of the Tasmanides, as determined by this study.

| Sample                       | Rock type    | Type   | Sm (ppm) | Nd (ppm) | $^{147}\text{Sm}/^{144}\text{Nd}$ | $^{143}\text{Nd}/^{144}\text{Nd}$ | $\pm 2\sigma$ | Age (Ma) | $^{143}\text{Nd}/^{144}\text{Nd}$ (t) | $\epsilon_{\text{Nd}}$ (t) |
|------------------------------|--------------|--------|----------|----------|-----------------------------------|-----------------------------------|---------------|----------|---------------------------------------|----------------------------|
| <i>Delamerian Orogen (E)</i> |              |        |          |          |                                   |                                   |               |          |                                       |                            |
| 9581                         | Tonalite     | I-type | 5.29     | 27.22    | 0.1176                            | 0.511918                          | 0.000015      | 515      | 0.511521                              | −8.85                      |
| CP6                          | Gabbro       | Mafic  | 5.73     | 25.56    | 0.1355                            | 0.512247                          | 0.000007      | 515      | 0.511790                              | −3.60                      |
| CP129                        | Gabbro       | Mafic  | 4.34     | 21.02    | 0.1247                            | 0.512147                          | 0.000011      | 515      | 0.511726                              | −4.85                      |
| 98-CP7                       | Diorite      | I-type | 3.62     | 17.67    | 0.1238                            | 0.512180                          | 0.000015      | 515      | 0.511762                              | −4.14                      |
| WAE3                         | Diorite      | I-type | 8.90     | 42.30    | 0.1272                            | 0.512143                          | 0.000011      | 510      | 0.511718                              | −5.13                      |
| WA3                          | Tonalite     | I-type | 9.62     | 39.33    | 0.1479                            | 0.512145                          | 0.000014      | 510      | 0.511651                              | −6.44                      |
| T2-135                       | Granodiorite | I-type | 3.71     | 21.22    | 0.1057                            | 0.511905                          | 0.000012      | 500      | 0.511559                              | −8.50                      |
| T2-318                       | Tonalite     | I-type | 3.49     | 20.11    | 0.1051                            | 0.511740                          | 0.000018      | 500      | 0.511396                              | −11.68                     |
| 97-299                       | Tonalite     | I-type | 3.21     | 17.87    | 0.1087                            | 0.511911                          | 0.000014      | 500      | 0.511555                              | −8.57                      |
| 98-13                        | Granodiorite | S-type | 2.09     | 7.41     | 0.1707                            | 0.512063                          | 0.000012      | 500      | 0.511504                              | −9.57                      |
| 98-27                        | Granodiorite | S-type | 1.79     | 6.28     | 0.1727                            | 0.512066                          | 0.000015      | 500      | 0.511500                              | −9.64                      |
| T2-302                       | Granodiorite | S-type | 3.34     | 16.15    | 0.125                             | 0.511936                          | 0.000015      | 500      | 0.511527                              | −9.12                      |
| 98-23                        | Granodiorite | S-type | 3.16     | 11.93    | 0.1599                            | 0.512069                          | 0.000009      | 500      | 0.511545                              | −8.76                      |
| 98-56                        | Granodiorite | S-type | 2.88     | 10.24    | 0.1698                            | 0.512113                          | 0.000013      | 500      | 0.511557                              | −8.53                      |
| 98-76                        | Granodiorite | S-type | 4.70     | 21.94    | 0.1295                            | 0.511959                          | 0.000015      | 500      | 0.511535                              | −8.96                      |
| 97-233                       | Granodiorite | S-type | 1.40     | 5.52     | 0.1536                            | 0.512060                          | 0.000010      | 500      | 0.511557                              | −8.53                      |
| T2-20                        | Tonalite     | S-type | 3.77     | 19.13    | 0.1190                            | 0.511919                          | 0.000013      | 500      | 0.511529                              | −9.07                      |
| 15583                        | Tonalite     | S-type | 4.94     | 23.42    | 0.1276                            | 0.511922                          | 0.000009      | 500      | 0.511504                              | −9.56                      |
| 15584                        | Tonalite     | S-type | 2.80     | 12.13    | 0.1395                            | 0.511950                          | 0.000014      | 500      | 0.511493                              | −9.78                      |
| 98-RC1                       | Diorite      | I-type | 9.05     | 50.37    | 0.1087                            | 0.512123                          | 0.000014      | 495      | 0.511771                              | −4.49                      |
| 9572                         | Granodiorite | I-type | 5.59     | 35.17    | 0.0961                            | 0.512128                          | 0.000013      | 495      | 0.511816                              | −3.59                      |
| 97-62                        | Granodiorite | I-type | 4.55     | 30.78    | 0.0893                            | 0.512100                          | 0.000013      | 495      | 0.511810                              | −3.71                      |
| 97-436                       | Granodiorite | I-type | 4.50     | 29.53    | 0.0922                            | 0.512159                          | 0.000010      | 495      | 0.511860                              | −2.74                      |
| 97-295                       | Granodiorite | I-type | 4.12     | 28.05    | 0.0887                            | 0.512057                          | 0.000012      | 495      | 0.511769                              | −4.51                      |
| <i>Lachlan Orogen (E)</i>    |              |        |          |          |                                   |                                   |               |          |                                       |                            |
| KK-2                         | Granodiorite | S-type | 5.63     | 27.30    | 0.1246                            | 0.512006                          | 0.000012      | 428      | 0.511657                              | −8.40                      |
| KK-25                        | Granodiorite | S-type | 5.82     | 29.55    | 0.1192                            | 0.511927                          | 0.000014      | 428      | 0.511593                              | −9.64                      |
| KK-16                        | Granodiorite | S-type | 6.05     | 30.05    | 0.1218                            | 0.511974                          | 0.000015      | 428      | 0.511633                              | −8.87                      |
| KK-10                        | Granodiorite | S-type | 5.79     | 28.17    | 0.1242                            | 0.511974                          | 0.000012      | 428      | 0.511626                              | −9.00                      |
| KB-115                       | Granodiorite | S-type | 6.16     | 30.85    | 0.1208                            | 0.511967                          | 0.000015      | 428      | 0.511628                              | −8.95                      |
| KB-9                         | Granite      | S-type | 5.26     | 24.70    | 0.1287                            | 0.512014                          | 0.000013      | 428      | 0.511653                              | −8.46                      |
| BB-106                       | Granodiorite | I-type | 3.92     | 21.57    | 0.1098                            | 0.512366                          | 0.000015      | 415      | 0.512068                              | −0.70                      |
| KK-21                        | Granodiorite | I-type | 2.52     | 14.59    | 0.1043                            | 0.512276                          | 0.000014      | 415      | 0.511993                              | −2.17                      |
| B4-28                        | Gabbro       | Mafic  | 1.25     | 5.52     | 0.1363                            | 0.512346                          | 0.000014      | 415      | 0.511976                              | −2.50                      |
| KK-9                         | Diorite      | I-type | 2.77     | 12.50    | 0.1338                            | 0.512257                          | 0.000013      | 415      | 0.511893                              | −4.10                      |
| KK-4                         | Tonalite     | I-type | 3.33     | 15.60    | 0.1289                            | 0.512187                          | 0.000014      | 415      | 0.511837                              | −5.21                      |
| KK-2b                        | Tonalite     | I-type | 2.64     | 12.41    | 0.1285                            | 0.512160                          | 0.000013      | 415      | 0.511811                              | −5.71                      |
| JTQ                          | Tonalite     | I-type | 3.53     | 17.45    | 0.1222                            | 0.512103                          | 0.000010      | 415      | 0.511771                              | −6.49                      |
| TKB-15B                      | Dolerite     | Mafic  | 6.93     | 34.71    | 0.1208                            | 0.512402                          | 0.000012      | 400      | 0.512086                              | −0.73                      |
| TKB-100                      | Tonalite     | I-type | 7.61     | 33.38    | 0.1378                            | 0.512149                          | 0.000011      | 400      | 0.511788                              | −6.54                      |
| TKB-74                       | Tonalite     | I-type | 4.58     | 19.76    | 0.1402                            | 0.512157                          | 0.000013      | 400      | 0.511790                              | −6.50                      |
| TKB-17                       | Tonalite     | I-type | 5.83     | 27.33    | 0.129                             | 0.512125                          | 0.000012      | 400      | 0.511787                              | −6.55                      |
| TKB-15F                      | Granite      | I-type | 3.32     | 18.45    | 0.1087                            | 0.512091                          | 0.000011      | 400      | 0.511806                              | −6.18                      |
| SCR-2                        | Diorite      | I-type | 2.56     | 11.38    | 0.1362                            | 0.512418                          | 0.000011      | 400      | 0.512061                              | −1.20                      |
| SCR-3                        | Diorite      | I-type | 1.48     | 6.73     | 0.1333                            | 0.512181                          | 0.000015      | 400      | 0.511832                              | −5.68                      |
| SCR-4                        | Diorite      | I-type | 1.56     | 7.02     | 0.1344                            | 0.512169                          | 0.000013      | 400      | 0.511817                              | −5.97                      |
| SCR-6                        | Diorite      | I-type | 0.88     | 3.50     | 0.1522                            | 0.512224                          | 0.000015      | 400      | 0.511825                              | −5.81                      |
| TKB-2                        | Diorite      | I-type | 4.54     | 27.38    | 0.1226                            | 0.51245                           | 0.000014      | 390      | 0.512137                              | 0.02                       |
| TKB-5                        | Diorite      | I-type | 4.03     | 19.04    | 0.1279                            | 0.512512                          | 0.000013      | 390      | 0.512185                              | 0.97                       |
| TKB-1                        | Tonalite     | I-type | 3.88     | 19.46    | 0.1206                            | 0.512474                          | 0.000014      | 390      | 0.512166                              | 0.59                       |
| TKB-6                        | Tonalite     | I-type | 3.87     | 19.88    | 0.1178                            | 0.512282                          | 0.000013      | 390      | 0.511981                              | −3.02                      |
| TKB-8                        | Granodiorite | I-type | 3.31     | 18.75    | 0.1068                            | 0.512410                          | 0.000014      | 390      | 0.512137                              | 0.03                       |
| TKB-11                       | Granite      | I-type | 2.97     | 16.82    | 0.1066                            | 0.512335                          | 0.000015      | 390      | 0.512063                              | −1.42                      |

(Table 2) was conducted by laser ablation multi-collector ICP-MS, using a Thermo-Scientific Neptune and 193 nm ArF laser. Data were acquired using spot sizes of 31  $\mu\text{m}$  to 58  $\mu\text{m}$  and a 4 Hz laser repetition rate. All oxygen and hafnium isotope data reported here derive from the melt-precipitated (emplacement age) portions of zircon crystals.

#### 4. The isotopic barcode of Tasmanide magmatism

The whole rock Nd and zircon Hf isotope compositions of the Tasmanide igneous units are summarised in Fig. 3. The data form a covariant array that lies above the bulk silicate Earth intersection and parallels the array defined by most crustal and mantle-derived rocks (Vervoort et al., 1999). This demonstrates the coherence of the

Tasmanide igneous system with regard to magma sources, and the lack of Hf–Nd isotope decoupling that can occur in certain sedimentary (Vervoort et al., 1999) and igneous (Schmitz et al., 2004) environments. When plotted as a function of crystallisation age, the zircon Hf–O isotope data define striking temporal trends that are mirrored by the whole rock Nd isotope compositions from a much larger number of samples (Fig. 4). A trend towards increasingly juvenile isotope compositions from the craton-proximal Delamerian orogen to the younger, outboard New England Orogen is evident for each granite type (Fig. 5). The agreement between the whole rock and zircon-derived datasets confirms that the zircons provide an unbiased isotopic record of silicic magmatism in the Tasmanides and thus, potentially, of crustal growth during orogenic evolution. The key

**Table 2**

Average hafnium and oxygen isotope data measured from melt-precipitated zircons of the Tasmanide igneous rocks during this study (quoted at 2 SD).

| Rock name/sample ID              | Type          | Age (Ma) | $^{176}\text{Hf}/^{177}\text{Hf}$ (t) (mean $\pm$ 2 SD) | $\epsilon_{\text{Hf}}$ (t) (mean $\pm$ 2 SD) | $\delta^{18}\text{O}$ (mean $\pm$ 2 SD) |
|----------------------------------|---------------|----------|---|--|---|
| <i>Delamerian Orogen (E)</i>     |               |          |   |  |   |
| Wando Tonalite 97-159            | I-type        | 515 Ma   | 0.282505 $\pm$ 37 (n = 17)                              | 1.90 $\pm$ 1.31                              | 6.47 $\pm$ 0.79 (n = 20)                |
| Warradale Tonalite 97-WA1        | I-type        | 510 Ma   | 0.282360 $\pm$ 54 (n = 11)                              | -3.33 $\pm$ 1.91                             | 7.28 $\pm$ 0.72 (n = 17)                |
| Tuloona Granodiorite 97-135      | I-S-type      | 500 Ma   | 0.282290 $\pm$ 29 (n = 8)                               | -6.03 $\pm$ 1.03                             | -                                       |
| Dergholm Granite B4-150          | A-type        | 488 Ma   | 0.282539 $\pm$ 85 (n = 14)                              | 2.56 $\pm$ 3.02                              | -                                       |
| <i>Lachlan Orogen (E)</i>        |               |          |   |  |   |
| Monzodiorite GOO103              | Macquarie arc | 484 Ma   | 0.282820 $\pm$ 28 (n = 19)                              | 12.35 $\pm$ 0.98                             | -                                       |
| Quartz diorite COH-8             | Macquarie arc | 457 Ma   | 0.282860 $\pm$ 01 (n = 3)                               | 13.20 $\pm$ 0.04                             | 5.21 $\pm$ 0.57 (n = 20)                |
| Monzodiorite GOO88               | Macquarie arc | 451 Ma   | 0.282797 $\pm$ 18 (n = 3)                               | 10.83 $\pm$ 0.62                             | -                                       |
| Monzonite CAD-35                 | Macquarie arc | 440 Ma   | 0.282799 $\pm$ 38 (n = 6)                               | 10.66 $\pm$ 1.34                             | -                                       |
| Monzonite CAD-54                 | Macquarie arc | 440 Ma   | 0.282801 $\pm$ 20 (n = 6)                               | 10.71 $\pm$ 0.70                             | -                                       |
| Monzonite GOO92                  | Macquarie arc | 439 Ma   | 0.282770 $\pm$ 22 (n = 26)                              | 9.62 $\pm$ 0.79                              | -                                       |
| Monzonite GOO96                  | Macquarie arc | 439 Ma   | 0.282776 $\pm$ 53 (n = 3)                               | 9.83 $\pm$ 1.87                              | -                                       |
| Hawkins Dacite HV-1              | S-type        | 430 Ma   | 0.282284 $\pm$ 67 (n = 23)                              | -7.79 $\pm$ 2.36                             | 9.14 $\pm$ 0.96 (n = 17)                |
| Cootralantra Granodiorite BB1    | S-type        | 430 Ma   | 0.282226 $\pm$ 68 (n = 12)                              | -9.86 $\pm$ 2.41                             | 8.36 $\pm$ 1.26 (n = 10)                |
| Arable Granodiorite BB3          | S-type        | 428 Ma   | 0.282235 $\pm$ 62 (n = 17)                              | -9.57 $\pm$ 2.16                             | 9.47 $\pm$ 1.13 (n = 14)                |
| Arable Granodiorite BB6          | S-type        | 428 Ma   | 0.282256 $\pm$ 85 (n = 14)                              | -8.81 $\pm$ 3.01                             | 8.37 $\pm$ 1.03 (n = 7)                 |
| Kadoona dacite Kdd-1             | I-type        | 414 Ma   | 0.282366 $\pm$ 25 (n = 48)                              | -5.27 $\pm$ 0.88                             | 7.24 $\pm$ 0.68 (n = 38)                |
| Glenbog Granodiorite TKG-1       | I-type        | 414 Ma   | 0.282372 $\pm$ 28 (n = 60)                              | -5.03 $\pm$ 0.98                             | 6.87 $\pm$ 0.65 (n = 47)                |
| Mumbulla Granite AB-118          | A-type        | 388 Ma   | 0.282565 $\pm$ 34 (n = 24)                              | 1.20 $\pm$ 1.14                              | -                                       |
| Watergums Granite G11            | A-type        | 388 Ma   | 0.282598 $\pm$ 99 (n = 26)                              | 2.44 $\pm$ 3.42                              | -                                       |
| Gilmore Hill granite 177         | I/A-type      | 375 Ma   | 0.282818 $\pm$ 28 (n = 18)                              | 9.90 $\pm$ 0.96                              | -                                       |
| Narraburra granite 178           | A-type        | 375 Ma   | 0.282838 $\pm$ 64 (n = 40)                              | 10.88 $\pm$ 2.28                             | 4.8 $\pm$ 1.04 (n = 12)                 |
| <i>New England Orogen (S)</i>    |               |          |   |  |   |
| Tia Granodiorite Y62             | S-type        | 302 Ma   | 0.282736 $\pm$ 45 (n = 12)                              | 5.37 $\pm$ 1.60                              | -                                       |
| Dundurabbin Granodiorite EA13    | S-type        | 290 Ma   | 0.282721 $\pm$ 58 (n = 2)                               | 4.59 $\pm$ 2.00                              | -                                       |
| Woolloomoombi Granodiorite EA8   | S-type        | 290 Ma   | 0.282687 $\pm$ 36 (n = 4)                               | 3.37 $\pm$ 1.30                              | -                                       |
| Banalasta Adamellite EA1         | S-type        | 292 Ma   | 0.282718 $\pm$ 56 (n = 6)                               | 4.52 $\pm$ 2.00                              | -                                       |
| Glencair Adamellite EA3          | S-type        | 288 Ma   | 0.282755 $\pm$ 27 (n = 2)                               | 5.72 $\pm$ 0.95                              | -                                       |
| Glenburnie Leucoadamellite 4055  | I-type        | 295 Ma   | 0.282845 $\pm$ 40 (n = 9)                               | 9.09 $\pm$ 1.43                              | -                                       |
| Barrington Tops Granodiorite MR1 | I-type        | 269 Ma   | 0.282924 $\pm$ 23 (n = 10)                              | 11.29 $\pm$ 0.81                             | -                                       |
| Mackenzie Adamellite 4047        | I-type        | 252 Ma   | 0.282802 $\pm$ 26 (n = 8)                               | 6.62 $\pm$ 0.93                              | -                                       |
| Duncan's Ck Trondhjemite EA25    | I-type        | 252 Ma   | 0.282916 $\pm$ 24 (n = 9)                               | 10.62 $\pm$ 0.85                             | -                                       |
| Duncan's Ck Trondhjemite EA27    | I-type        | 249 Ma   | 0.282902 $\pm$ 15 (n = 6)                               | 10.06 $\pm$ 0.53                             | -                                       |

Individual analyses are listed in supplementary Tables 1 and 2.

difference between the whole rock and zircon data is that the latter are more suitable for evaluating relative contributions from mantle and crustal sources (e.g. Kemp et al., 2007).

Epsilon Hf values in the Delamerian-aged zircons (Figs. 4b and 5) change from weakly positive for the oldest hornblende tonalites, through to strongly negative for syn-compressional peraluminous

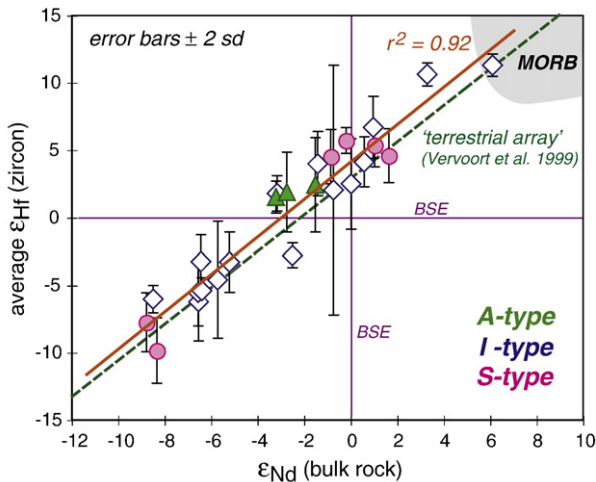


**Fig. 3.** Plot of bulk rock  $\epsilon_{\text{Nd}}$  versus average zircon  $\epsilon_{\text{Hf}}$  (error bars at 2 standard deviations) for igneous units of the Tasmanides. The 'terrestrial array' and the field of mid-ocean ridge basalts (MORB) are from Vervoort et al. (1999).

granodiorites, and eventually returning to positive values in the post-compressional A-type granites. The hornblende tonalites are coeval with hornblende gabbros and high-Mg diorites, and formed above a west-dipping subduction zone (Kemp, 2003; Foden et al., 2006). The same tectonic setting and arc polarity is inferred for coeval, geochemically analogous mafic rocks emplaced in the formerly contiguous Ross orogen in Antarctica (Tiepolo and Tribuzio, 2008). Zircon  $\delta^{18}\text{O}$  data for the Delamerian hornblende tonalites are elevated compared to mantle values (Fig. 4c), indicating a significant supracrustal contribution. The unradiogenic  $\epsilon_{\text{Hf}}$  of the granodiorite zircon suggests a larger metasedimentary input, according with its peraluminous chemistry and with transitional field contacts with migmatitic gneisses (Kemp et al., 2002). Much higher  $\epsilon_{\text{Nd}}$  and zircon  $\epsilon_{\text{Hf}}$  of the A-type granites indicate a switch to relatively juvenile (i.e. more mantle-like) felsic magma sources after the cessation of convergent deformation.

The V-shaped Delamerian  $\epsilon_{\text{Hf}}$ -time pattern is duplicated in the slightly younger Lachlan Orogen. Zircons from the Macquarie arc intrusives (484–439 Ma) are isotopically primitive, with  $\epsilon_{\text{Hf}}$  values that fall within the range shown by modern subduction-related basalts (typically +15 to +5, Vervoort et al., 1999; Fig. 4b). However, the onset of voluminous felsic magmatism at ~430 Ma involved a dramatic and abrupt decrease in whole rock  $\epsilon_{\text{Nd}}$  and zircon  $\epsilon_{\text{Hf}}$ , and an increase in zircon  $\delta^{18}\text{O}$  towards sediment-like values (see Fig. 4). These features signal the fusion of Ordovician metasedimentary units to generate cordierite-rich S-type granites and their volcanic equivalents. Elevated whole rock  $\delta^{18}\text{O}$  and generally negative  $\epsilon_{\text{Nd}}$  values suggest that metasedimentary materials also contributed to the younger I-type intrusives (McCulloch and Chappell, 1982; Gray, 1984). The complex interplay between juvenile and metasedimentary sources during the formation of the Lachlan I-type

magmas is manifest by zircon  $\delta^{18}\text{O}$ – $\epsilon_{\text{Hf}}$  arrays (Kemp et al., 2007). However, the whole rock  $\epsilon_{\text{Nd}}$  and zircon  $\epsilon_{\text{Hf}}$  values of the I-type rocks rise progressively with decreasing age, accompanied by a fall in average zircon  $\delta^{18}\text{O}$ . This trend is continued by the A-type plutons, which eventually acquire depleted-mantle-like isotope character in the youngest, peralkaline samples (Kemp et al., 2005).

The emplacement of Carboniferous S-type granites in the New England Orogen signals a return to lower whole rock  $\epsilon_{\text{Nd}}$ . Nevertheless, and despite the strongly elevated  $\delta^{18}\text{O}$  (to 13‰, O’Neil et al., 1977), these rocks have distinctly juvenile Nd–Hf isotope compositions compared to the Lachlan and Delamerian S-types (Figs. 4 and 5). Zircon  $\epsilon_{\text{Hf}}$  values (to +6) are the highest yet reported for S-type granites. Likewise, whole rock  $\epsilon_{\text{Nd}}$  and zircon  $\epsilon_{\text{Hf}}$  values of the I-type granites are dominantly positive and dispersed between CHUR and depleted mantle values. Zircon  $\epsilon_{\text{Hf}}$  variability within individual samples is also far less pronounced than is the case for the older Tasmanide granites. Combined, these features suggest derivation of the New England plutons from juvenile crustal or mantle protoliths of limited isotopic heterogeneity.

In summary, the isotope–time pattern of Tasmanide magmatism shows three abrupt decreases in whole rock  $\epsilon_{\text{Nd}}$  and zircon  $\epsilon_{\text{Hf}}$ , which precede the main episode of felsic magmatism in each orogen. A

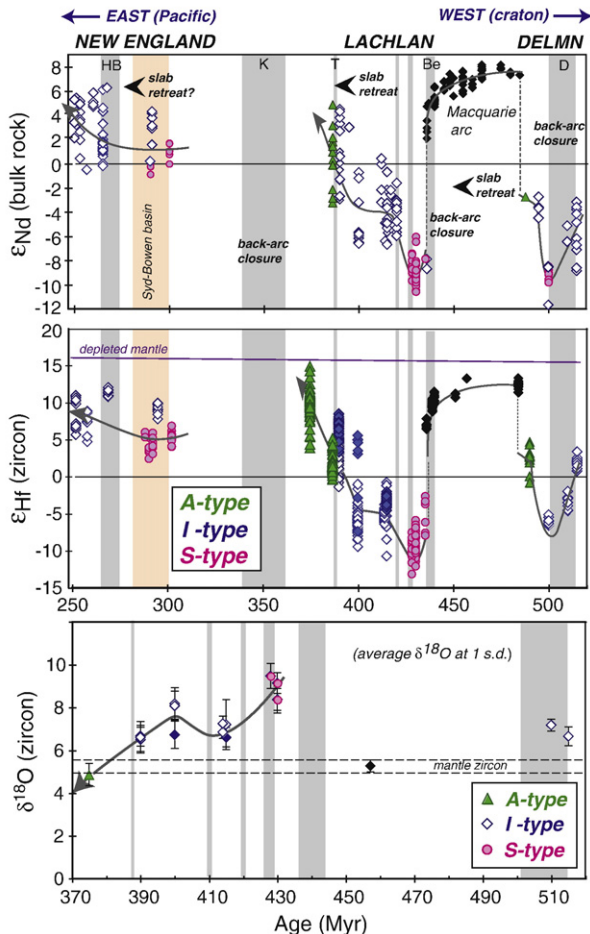


**Fig. 4.** Isotope and tectono-magmatic evolution of the Tasmanides defined by (a) the  $\epsilon_{\text{Nd}}$  values of igneous rocks, (b)  $\epsilon_{\text{Hf}}$  values of granite-hosted zircons, and (c) average  $\delta^{18}\text{O}$  of granite-hosted zircons (with 1 SD error bars; note the different time scale). Data sources are as for Fig. 2 but including Belousova et al., 2006; Kemp et al., 2005, 2007; and Fu et al., 2009). Filled diamonds on the  $\epsilon_{\text{Hf}}$ –time panel represent analyses from dioritic–gabbroic units. The shaded time slices correspond to major contractional episodes, as follows: HB, Hunter–Bowen; K, Kanimblan; T, Tabberabberan; Bo, Bowning; Be, Benambran (early phase); D, Delamerian. The timing of these events is taken from Landenberger et al. (1995), Collins and Hobbs (2001), Collins (2002a,b), Gray and Foster (2004), Foden et al. (2006) and Cawood and Buchan (2007).

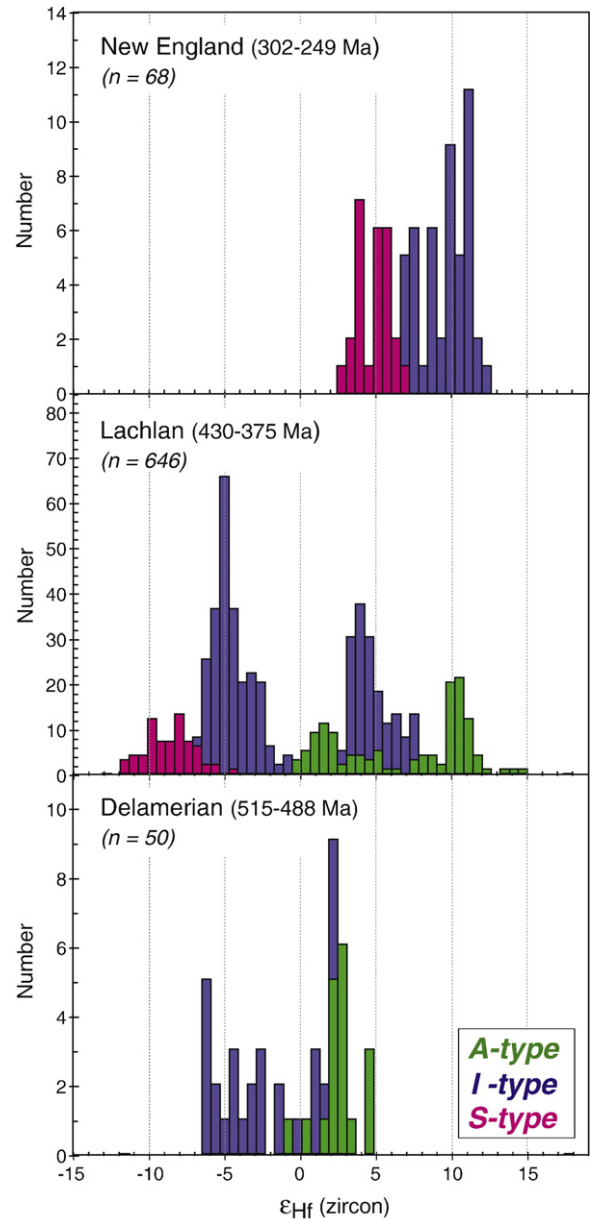


**Fig. 5.** Histograms of zircon  $\epsilon_{\text{Hf}}(t)$  values for granitic rocks of the Delamerian, Lachlan and New England orogens. The bimodal distribution for the Lachlan I-type granites corresponds to rocks with abundant zircon inheritance (low  $\epsilon_{\text{Hf}}$  peak) and sparse inheritance (high  $\epsilon_{\text{Hf}}$  peak).

fourth, smaller decrease occurs near 400 Ma. These inflections, marked by S-type granite emplacement, are superimposed upon a general trend towards increasingly radiogenic Nd–Hf isotope ratios shown by igneous rocks with decreasing age, and from west to east. The isotope–time trends correlate with the pattern of compressional and extensional events in the Tasmanides (Fig. 4), suggesting a feedback between tectonic activity and magma source. The significance of these observations is explored below.

## 5. Discussion

### 5.1. Relating Nd–Hf–O isotope changes to tectonic evolution

The orogenic history of the Tasmanides is characterised by episodes of extension and sedimentation that are punctuated by brief (<15 Ma) contractional events, all of which accord with the

progressive oceanward migration of a west-dipping subduction zone (Collins 2002a; Gray and Foster, 2004; Cawood and Buchan, 2007). Collins (2002b) attributed the main contractional periods to back-arc closure events coinciding with the arrival of buoyant oceanic lithosphere at the trench, causing flat subduction and a transient inboard advance of the slab hinge. During this time the turbidite package deposited in the antecedent back-arc basin is thickened and thrust to mid-crustal depths. Arc magmatism reasserts once the oceanic anomaly is subducted, leading to pronounced trench rollback, upper plate extension and the formation of a younger rift basin outboard of the new fold and thrust belt (Collins, 2002a,b; Collins and Richards, 2008). Igneous activity thus migrates outboard from the older, thickened back-arc into the new back-arc extension zone and arc front as the slab hinge retreats oceanward.

Implicit within this ‘tectonic switching’ scenario are changes in the availability and composition of magma sources throughout orogenic evolution. Such changes should manifest in the isotope record of igneous rocks, and form the basis for testing the model. Specifically, the model of Collins (2002a,b) predicts – (1) a greater crustal contribution to arc magmas during incipient back-arc closure and lithospheric thickening, (2) extensive reworking of metasedimentary units once subduction re-initiates beneath the old, thickened back-arc basin, and (3) a return to primitive isotope compositions as subduction zone magmatism moves outboard of thickened crust during renewed slab rollback. This cycle should be repeated during the history of the orogen.

Evidence for these three features is indeed present in the isotope–time patterns in Fig. 4. First, the isotopic response to back-arc closure is conspicuous in the igneous rocks formed during the terminal stages of oceanic arc evolution. The zircon  $\epsilon_{\text{Hf}}$  and whole rock  $\epsilon_{\text{Nd}}$  become clearly less radiogenic from 460 to 440 Ma in the Macquarie arc, implying greater crustal input into these magmas during the early stages of lithospheric thickening (Crawford et al., 2007). The oldest Delamerian hornblende tonalites show a similar trend. Enhanced crustal input could have occurred by – (1) increased sediment subduction, (2) greater subduction erosion as the slab angle decreased, delivering accretionary prism materials to beneath the arc (e.g. Clift and Vannuchi, 2004), or (3) contamination of the arc magmas during their passage through the thickened turbidite sequence. The last of these probably contributes to the Delamerian trend since the decreasing zircon  $\epsilon_{\text{Hf}}$  was accompanied by increasing zircon  $\delta^{18}\text{O}$ .

Second, crustal reworking after back-arc closure is registered by the marked decrease in  $\epsilon_{\text{Nd}}$  and zircon  $\epsilon_{\text{Hf}}$  that closely follow major crustal thickening episodes in each Tasmanide terrane (Fig. 4). These inflections signify the emplacement of S-type granites formed largely from metasedimentary precursors (White and Chappell, 1977). S-type magma formation was conceivably facilitated by basaltic ingress as subduction recommenced, whereby the pulse of heat and fluid from crystallising hydrous arc magmas triggered rapid melting of metasedimentary crust that was thickened during the previous back-arc inversion (Collins and Richards, 2008). Supporting this, the Tasmanide S-type granites are coeval with mafic intrusives of subduction affinity (Kemp, 2003; Healy et al., 2004). The short time delay between crustal thickening and S-type magma generation is also consistent with the back-arc region remaining hot during extensional and compressional modes (Hyndman et al., 2005). S-type granites are not associated with the dip in the isotope–time pattern near 400 Ma. However, I-type tonalites emplaced at this time have  $^{18}\text{O}$ -enriched zircons ( $\delta^{18}\text{O} > 8\%$ ) that fingerprint extensive sediment incorporation (Kemp et al., 2007), and are mingled with basalts that have arc-like chemical signatures. These features imply a weak compressional event in the eastern Lachlan associated with transient arc incursion at 400 Ma.

Third, the predicted transition to mantle-like isotope compositions after subduction re-initiation and renewed arc retreat is evident with the increasing  $\epsilon_{\text{Nd}}$  and  $\epsilon_{\text{Hf}}$  shown by igneous rocks of the three orogens, and the accompanying change from peraluminous S-type to

metaluminous I-type chemistry. A waning metasedimentary contribution to the magmas is an obvious explanation for this trend. This could reflect both thinning of the metasedimentary sequence during extension (Collins and Richards, 2008) and thermal maturation of the arc–back-arc crust with ongoing subduction and mafic underplating, whereby greater amounts of silicic liquid are generated by crystallisation of successively underplated basaltic sills (Annen and Sparks, 2002).

## 5.2. Secular change in mantle sources

Besides differing proportions of magma source materials, the temporal isotope trends shown by the Tasmanide granites also reflect a change in the nature of the coeval mantle-derived component as the orogen developed. In the Lachlan, secular evolution in mantle sources is suggested by (1) a transition in mafic rock geochemistry from arc-like at 430 Ma to intraplate-like by 375 Ma (Collins, 2002b), and (2) by the increasingly radiogenic Nd and Hf isotope compositions of mafic intrusives (Figs. 4 and 6), which approach depleted mantle-like values by 390 Ma and mirror the increasingly radiogenic  $\epsilon_{\text{Nd}}$  and zircon  $\epsilon_{\text{Hf}}$  of I-type granites over this period. The mafic rock isotope trends cannot easily be explained by decreasing contamination in the crust, since zircons in gabbros that have low  $\epsilon_{\text{Hf}}$  also have mantle-like  $\delta^{18}\text{O}$  (Kemp et al., 2007). Alternatively, given that  $\epsilon_{\text{Nd}}$  correlates with indices of contributions from the subducted slab (Fig. 6), the mafic intrusives may be recording a diminishing subduction-induced enrichment in the mantle source with time, as consistent with the envisaged oceanward migration of the subduction zone (Collins, 2002b; Gray and Foster, 2004). The terminal phase of mafic magmatism in the Lachlan orogen is represented by alkaline, intraplate-like basalts with depleted mantle isotope signatures (Fig. 6), which intruded after crustal thickening at 390 Ma. These rocks, which reflect small degree melting of pristine asthenosphere, were emplaced in intra-continental rifts (effectively far-field back-arc basins) that formed >100 km behind the contemporary locus of intra-oceanic arc magmatism in the nascent New England orogen.

An analogous isotope progression is evident for mafic intrusives of the eastern Delamerian orogen. The oldest metabasalts are alkalic to MORB-like ( $\epsilon_{\text{Nd}}$  to +5.3; Turner et al., 1993), reflecting an early extensional period. Calc-alkaline hornblende gabbros and high-Mg diorites formed during arc–craton convergence from 515 to 500 Ma show less radiogenic Nd isotope compositions ( $\epsilon_{\text{Nd}}$  –3 to –5), consistent with generation from mantle with a strong slab-derived

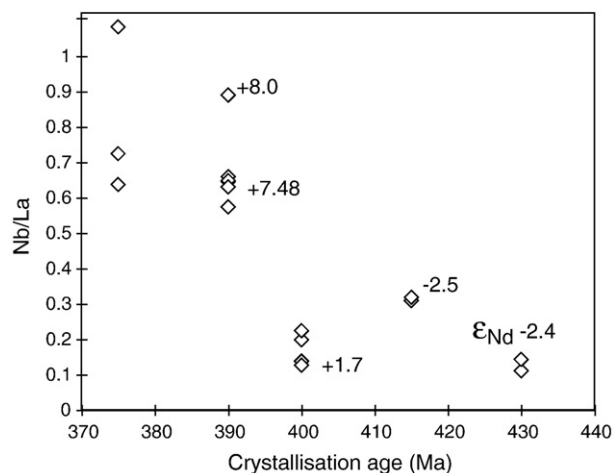


Fig. 6. Nb/La ratios of mafic rocks from the eastern Lachlan Orogen plotted as a function of emplacement age. The Nd isotope composition of individual samples is also shown. Data are from Keay et al. (1997), Healy et al. (2004), Wormald et al. (2004), and this study.

enrichment, or with contamination from the thickened turbidites. A crustal component is less obvious within tholeiitic dolerites and gabbros emplaced after major compression, which show a return to higher  $\epsilon_{\text{Nd}}$  (up to +4; Turner, 1996). These chemical and isotopic features are also compatible with arc retreat.

### 5.3. The transition to A-type magmatism

I-type magmatism in the three Tasmanide terranes was supplanted by emplacement of A-type granitic-volcanic rocks (Turner et al., 1992; Landenberger and Collins, 1996; Wormald et al., 2004). A-type granites in the Delamerian and Lachlan orogens are closely associated with post-compressional mafic intrusives that have similar geochemical and isotopic characteristics to the granites (see Turner et al., 1992, Kemp et al., 2005). Turner et al. (1992) therefore suggested that the Delamerian A-type granites originated through >90% crystallisation of a tholeiitic basaltic precursor represented by coeval gabbros, which is supported by the juvenile  $\epsilon_{\text{Nd}}$  and zircon  $\epsilon_{\text{Hf}}$  values of the A-types compared to many of the older I-type rocks (Fig. 4). Similarly, the volumetrically-minor Lachlan A-types are inferred to have differentiated from alkaline basaltic magmas, with trends to lower zircon  $\epsilon_{\text{Hf}}$  and sparse inherited zircon cores reflecting variable incorporation of crust (Fig. 4; Kemp et al., 2005). The retention of depleted mantle-like Hf isotope ratios and mantle-like  $\delta^{18}\text{O}$  in the youngest, peralkaline Lachlan A-type plutons (Fig. 4) implies that these magmas traversed dominantly young igneous crust, and/or crust that was thinned during localised rifting.

The transition from I- to A-type magmatism in the Delamerian and Lachlan orogens was evidently controlled by the switch from hydrous arc magmas to intraplate-like (i.e. less hydrous) tholeiitic-alkaline basalts, which in turn is linked to slab rollback after contractional deformation. A-type magmatism therefore marked the transition to an intraplate setting during the evolution of the Delamerian and Lachlan orogens, with the establishment of a new outboard oceanic arc system (i.e. the Macquarie arc after 490 Ma, and the Gympie arc of the New England orogen after 375 Ma) and the beginning of a new orogenic cycle.

### 5.4. Tectonic controls on isotopic differences between orogens

Tectonic switching appears capable of reconciling the complex isotope–time patterns defined by the Tasmanide igneous rocks. In this model, trends towards decreasing  $\epsilon_{\text{Hf}}$  and  $\epsilon_{\text{Nd}}$  reflect enhanced crustal reworking attending arc compression and lithospheric thickening, whereas the subsequent progression to juvenile isotope signatures manifests the switch to an extensional mode induced by arc retreat. This cycle is repeated in the Delamerian, Lachlan and New England Orogens, as the subduction zone migrated oceanward.

Nevertheless there are isotopic differences between the three Tasmanide terranes (Fig. 5). An obvious contrast concerns the juvenile character of the New England granites, and the muted zircon  $\epsilon_{\text{Hf}}$  variation within individual samples, compared to granites of the Lachlan and Delamerian orogens. This cannot be attributed to lesser degrees of metasedimentary reworking, since the presence of S-type granites, Sr–Nd isotope arrays (Fig. 2) and I-types with elevated  $\delta^{18}\text{O}$  (7.7–10‰, O'Neil et al., 1977) and depleted  $\delta^7\text{Li}$  (Bryant et al., 2004) confirm the importance of this process in the New England orogen. Rather, the difference reflects the juvenile nature of the sedimentary component incorporated by the New England granites, and thus the minor isotope contrast between supracrustal and mantle-derived source components in this area (see Fig. 2). The sedimentary substrate to the New England orogen comprises part of a Silurian to Carboniferous accretionary prism and contains detritus from a primitive oceanic to continental volcanic arc that was active through the Early to Mid-Paleozoic (Hensel et al., 1985). S-type granites of the area thus inherited the radiogenic whole rock  $\epsilon_{\text{Nd}}$  and zircon  $\epsilon_{\text{Hf}}$

signature from this young sedimentary provenance. In contrast, the Cambrian to Ordovician turbidites of the Delamerian and Lachlan orogens were shed from cratonic sources of substantial crustal residence ages, as suggested by the strongly negative whole rock  $\epsilon_{\text{Nd}}$  values, together with the U–Pb age spectra (Ireland et al., 1998) and Hf isotope composition (Kemp et al., 2006) of detrital zircons. Sedimentary reworking thus leaves a greater Nd–Hf isotopic imprint on I-type granites of the Lachlan and Delamerian orogens than those of New England.

Another difference relates to the shape of the isotope–time patterns after major thickening events. The clear trend towards increasing  $\epsilon_{\text{Nd}}$  and zircon  $\epsilon_{\text{Hf}}$  shown by the Lachlan granites after 430 Ma conceivably reflects continuing magmatism during protracted extension, spanning 50 Myr. A similar trend occurs in the Delamerian orogen after 500 Ma, but the progression from I-type to A-type occurs over a shorter duration (<15 Myr). Moreover, in contrast to the Lachlan, A-type magmatism in the Delamerian orogen is more voluminous than the earlier I-type plutonism (Turner et al., 1992). The tholeiitic affinity of the post-compressional Delamerian mafic plutons (Turner, 1996) also implies a greater degree of mantle melting, and thus extension, than was responsible for the alkaline dykes associated with the small volume Lachlan A-types (e.g. Collins, 2002a, b; Wormald et al., 2004). Turner (1996) attribute the generation of the Delamerian A-type magmas to convective removal of lithospheric mantle, allowing asthenospheric upwelling and melting of enriched mantle domains to produce the basaltic precursors to the A-type granites. An alternative is that the requisite extension for extensive mantle melting and A-type generation was caused by a short, but pronounced phase of slab retreat after crustal thickening at 500 Ma. The latter scenario is compatible with the postulated abrupt shift in the locus of contemporary arc magmatism from the Jamieson–Licola arc in eastern Victoria to the Macquarie arc in central NSW (presently a distance of 200 km, as in Fig. 1, potentially greater prior to tectonic shortening) in about 10 Myr (e.g. Foster et al., 2005). One implication is that the rate of isotopic change after thickening events, and the volume of post-convergent magmatism, may reflect the rapidity of arc retreat following the resumption of subduction, although other factors, such as the strength and/or degree of structural anisotropy in the rock package being rifted, may also be important.

In this respect, it is notable that there is less evidence for a systematic isotope–time progression over the 70 Myr magmatic history of the New England orogen, besides the younger I-type intrusives having on average higher  $^{143}\text{Nd}/^{144}\text{Nd}$  and zircon  $^{176}\text{Hf}/^{177}\text{Hf}$  than the S-types. Instead, the range of isotope compositions shown by the I-types suggests ongoing incorporation of accretionary prism or meta-igneous arc basement by juvenile magmas. This is difficult to reconcile with arc extension and lithospheric thinning during slab retreat, which should diminish the capacity of older crust to contribute to silicic magmas with time. The irregular  $\epsilon_{\text{Nd}}$ –time pattern shown by the New England I-type granites might instead be typical of plutonic belts formed above quasi-stationary subduction zones that oscillated between extensional and compressional regimes. Similar trends occur within other juvenile supra-subduction zone igneous belts, such as those of the Canadian Cordillera (Samson et al., 1989).

### 5.5. Tectonic controls on crust generation

An important aim of this study is to ascertain the amount of new crust formed at different stages during the evolution of the Tasmanides, and thus to identify the tectonic circumstances that promote the generation of continental crust. In detail, this requires quantification of the total mantle to crust flux during this ~290 Ma period, including that comprising the Cambrian–Ordovician oceanic arc basement formed by subduction zone retreat, and the basaltic underplate formed during subsequent magmatic episodes. Although now largely buried beneath younger geological units, seismic profiles

suggest that Cambrian–Ordovician and probably younger mafic rocks dominate the middle to lower crust in eastern Australia (e.g., Glen et al., 2002), but the various age components are difficult to distinguish unambiguously. An alternative approach is to track juvenile input into granitic plutons, specifically to quantify the young mantle-derived component of these magmas and to use this as a proxy for continental growth at different time periods. The exercise is best suited to the eastern Lachlan orogen, where the most comprehensive zircon isotope dataset for granitic and associated mafic rocks exists.

The average proportion of new crust incorporated by igneous suites of the eastern Lachlan Orogen can be estimated by isotope mixture modelling (Fig. 7). This assumes that the formation of these granites involved interaction between juvenile mantle-derived and crustal sources, as supported by a large body of field, geochemical and isotope evidence (e.g. Gray, 1984; Collins, 1998; Keay et al., 1997; Maas et al., 1997; Waight et al., 2001; Healy et al., 2004; Belousova et al., 2006; Kemp et al., 2005, 2007, 2008). In most cases, local mafic intrusives are isotopically suitable proxies for juvenile end-members (Keay et al., 1997; Healy et al., 2004; Collins et al., 2006; Kemp et al., 2007), whereas a metasedimentary composition similar to that of the Ordovician country rock approximates the crustal ingredient (e.g. Gray, 1984). Besides these components, the role of meta-igneous crust (e.g. White and Chappell, 1977) as a granitic source is difficult to evaluate. Plausible candidates include the Cambrian arc–back-arc

substrate to the turbidites (Keay et al., 1997) and the products of Ordovician oceanic arc magmatism. However, because this material was newly formed during the evolution of the Tasmanides, its incorporation into granitic magmas still represents the addition of juvenile continental crust.

Fig. 7 shows that the inferred fraction of juvenile crust incorporated by felsic igneous suites of the eastern Lachlan Orogen increases with decreasing emplacement age, in concert with the isotope–time trends (Fig. 4). However, the outcrop area of these rocks steadily declines, most markedly for the post-compressional A-type granites. If the outcrop area relates generally to magmatic productivity, as implied by the large differences in surface area for suites of different age, then the most significant period of Siluro–Devonian crust formation in the Lachlan immediately followed crustal thickening and back-arc closure. This links high rates of crust generation to subduction re-initiation and arc retreat. Fig. 7 also reveals that much new continental crust formed during S-type magmatism, despite the perception that S-type rocks form predominantly through intra-crustal reworking. We speculate that the falling rate of crust generation late in the orogenic history was due to rapid slab rollback combined with progressive lithospheric thickening, inhibiting decompressive mantle melting and thus basaltic input into the crust.

Extending these calculations to the Delamerian and New England orogens awaits isotopic characterisation of the juvenile components in these areas. However, some general comments are possible. First, the fraction of mantle-derived melt in the Delamerian and New England S-types is evidently much less than that inferred for the Lachlan S-types, as suggested by the almost complete overlap between the Sr–Nd isotope fields of the S-type granites and metasedimentary basement in these areas (Fig. 2). This probably reflects the greater fertility to melt production of the feldspathic, first-cycle metasedimentary rocks in the Delamerian and New England orogens compared to that of the quartz-rich Lachlan turbidites. The Delamerian and New England metasedimentary units would therefore be more capable of yielding mobile felsic magmas without augmentation from a juvenile component.

Second, due to the relatively large volume and basaltic heritage, A-type magmatism in the Delamerian orogen involved considerably greater crustal growth than A-type emplacement in the Lachlan orogen. The Delamerian A-type granites occupy the same Sr–Nd isotope field as their inferred mafic magmatic parents, and if this range reflects mantle heterogeneity (Turner, 1996), then the A-types represent entirely juvenile continental additions (Turner et al., 1992). The proportion of new crust falls to 85–90% if the Sr–Nd isotope array is due to incorporation of metasedimentary material (Foden et al., 2002), but remains significant. As in the Lachlan, juvenile crust production associated with Delamerian granitic magmatism peaked shortly after a major compressional phase.

Thirdly, the whole rock and zircon-derived isotope data indicate that the New England Orogen comprises juvenile continental crust with very little reworked cratonic material. The diminished cratonic input reflects pronounced subduction zone retreat and formation of the New England orogen in an arc-proximal environment well outboard of the ancient Gondwana margin (Fig. 1). Juvenile zircon  $\epsilon_{\text{Hf}}-\delta^{18}\text{O}$  systematics are also shown by Cretaceous granitic intrusives of New Zealand (Bolhar et al., 2008) that formed in a continental arc setting south and east of the New England orogen exposed on mainland Australia.

### 5.6. Supercontinents, subduction systems and rapid continental growth

The development of the Tasmanides coincided with the inception of an outboard subduction zone during the final phases of amalgamation of the East and West Gondwana cratons (Cawood and Buchan 2007). The oceanward retreat of this arc system formed the eastern third of Australia in less than 300 Myr, and the isotopic data suggest that a substantial proportion of this crust is juvenile. It is possible to

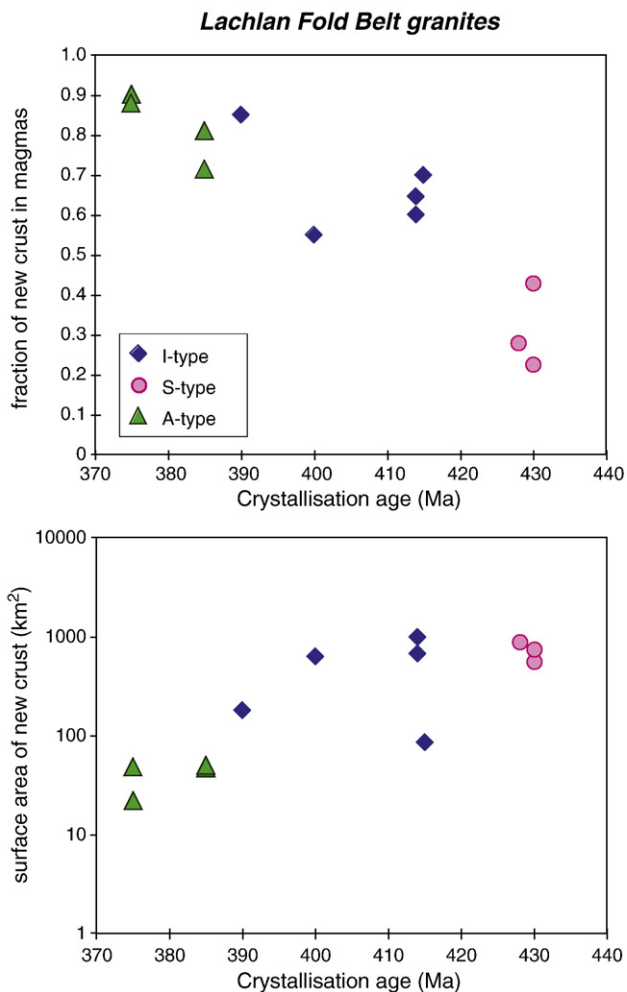


Fig. 7. The model fraction of juvenile crustal material incorporated by the eastern Lachlan granite suites (top) and the surface area occupied by this new continental crust (bottom). Details of the calculations are provided in the supplementary data.

estimate the rate of crust generation in the Tasmanides, assuming that the southern part of the orogen on mainland Australia formed entirely in response to Cambrian to Triassic magmatism. Adopting an average present-day crustal thickness of 40 km (e.g. Glen et al., 2002), and after subtraction of a 15 km thickness of craton-derived metasedimentary rock, then the crustal addition rate for the southern Tasmanides is  $70 \text{ km}^3/\text{km}/\text{Ma}$  for an arc strike length of 1200 km and magmatic history of 285 Ma, or just under  $0.09 \text{ km}^3/\text{a}$ . This conservative estimate resembles the average magmatic productivity at modern convergent plate boundaries ( $87 \text{ km}^3/\text{km}/\text{Ma}$ ), and, in terms of net crustal growth rate, is only exceeded by Java ( $0.132 \text{ km}^3/\text{a}$ ), the Marianas ( $0.134 \text{ km}^3/\text{a}$ ) and the Solomons ( $0.101 \text{ km}^3/\text{a}$ ) (figures from Clift and Vannuchi, 2004).

Accretionary orogenesis as described for eastern Australia provides an effective mechanism for rapid crust formation in subduction settings that complements traditional models of supra-subduction zone arc magmatism (e.g. Davidson and Arculus, 2006). In the Tasmanides, the craton-derived turbidite blanket that accumulated in back-arc basins from the Early Cambrian to Late Devonian also played a key role in continental growth. On the one hand, the remelting and ingestion of these materials by mafic magmas camouflaged the isotopic evidence for crust formation associated with magmatic episodes. However, this crustal reworking process was fundamental to granite production and thus to the differentiation, stabilisation and preservation of juvenile continental crust. Provenance studies suggest that sedimentary detritus was derived from further south along the Paleo-Pacific Gondwana margin (Ireland et al., 1998; Fergusson and Fanning, 2002), presumably from rapid denudation of collision-related mountain belts. Plate reorganisation associated with supercontinent assembly therefore not only triggered a geodynamic regime that promoted crustal growth, but supplied sediment to the newly formed back-arc basins that helped stabilise the new arc crust.

How important was continent formation in the Tasmanides in a global context? Age histograms of isotopically juvenile igneous rocks (Condie, 1998) show no large peaks after 1.2 Ga but such compilations inherently neglect the latent mantle components of granitic rocks where crustal reworking was also important (as in the Tasmanides), as well as mafic additions to the lower-middle crust during times of granite generation. Jahn et al. (2000) present Nd isotopic evidence for substantial Phanerozoic continental growth in the Central Asia Orogenic Belt, whose formation was broadly contemporaneous with the Tasmanides. An enriched mantle component with unradiogenic Nd isotope characteristics has been postulated for other Paleozoic orogens, including the Variscan (Gerdes et al., 2000) and North American Cordillera (Coleman et al., 1992), suggesting that crust formation may not always be detectable through depleted mantle-like isotope signatures. A significant Phanerozoic mantle depletion event is, however, yet to be recognised in the  $^4\text{He}/^3\text{He}$  and Re–Os isotope systematics of mantle-derived igneous rocks (Parman, 2007; Pearson et al., 2007). This suggests either that crust extraction was comparatively unimportant during this period, or (for Re–Os) that the evidence was erased from the mantle record by higher rates of crustal recycling at Phanerozoic subduction zones.

Nevertheless, the geodynamic mechanism that formed the Tasmanides may also have driven rapid continental growth in ancient orogens. For example, there are many geological similarities between the Tasmanides and the vast 1.9–1.5 Ga orogens of cratonic Australia, which formed during a global pulse of crustal growth (Condie, 1998). These similarities include a turbidite-dominated basement, voluminous felsic magmatism, episodic high T–low P metamorphism, and a protracted orogenic history involving alternating extension and contraction (see Myers et al., 1996). These are hallmark features of Phanerozoic accretionary orogens (Cawood, 2005). Similarly, the Trans-Hudson orogen of Canada (1.92–1.81 Ga) contains remnant juvenile oceanic arc sequences and thick turbidite sequences that

were deposited in back-arcs and overprinted by high T, low P metamorphism broadly coeval with gabbro-granite intrusion (e.g. Ansdell et al., 1995; Hollings and Ansdell, 2002). The early (pre-collisional) history of this orogen involved arc accretionary processes, in part behind a retreating subduction boundary (Ansdell et al., 1995). These Proterozoic examples show that rapid ancient continental growth can be explained by subduction and perhaps slab retreat without recourse to slab avalanches or mantle superplumes.

## 6. Conclusions

Isotope–time trends defined by igneous rocks of eastern Australia manifest the interplay between tectonic activity and magma source in an evolving accretionary orogen. We attribute the cyclic secular trends in bulk rock  $\varepsilon_{\text{Nd}}$  and zircon  $\varepsilon_{\text{Hf}}-\delta^{18}\text{O}$  to variable incorporation of older, dominantly metasedimentary, crust during alternating regimes of contractional and extensional tectonics behind a retreating subduction zone. Most critically, the steady progression to radiogenic Nd–Hf isotope signatures after crustal thickening episodes reflects an enhanced juvenile magmatic input as the arc reverts to an extensional, back-arc rifting mode upon the re-initiation of slab retreat. Interaction between juvenile magma and sedimentary units deposited during prior back-arc rifting was integral to the production of differentiated (granitic) crust that has high preservation potential in the geological record; this emphasises the significance of back-arc environments for continental growth. The juvenile component within the Tasmanide granites increased with time and from west to east, being highest in the outboard New England orogen, which contains minimal craton-derived detritus. If the present-day oceanic elements of the Tasmanides, represented by the Tonga–Kermadec arc–back-arc systems, were eventually accreted to eastern Australia then these would represent almost entirely juvenile additions.

The Tasmanide case study highlights the utility of isotopic signals in igneous rocks for tracing or evaluating tectonic processes, given that the latter regulate the composition and availability of magma sources (see also Draut and Clift, 2001; Murphy and Nance, 2002). More widely, using isotopes to link juvenile input and tectonic environment in a range of orogenic systems can provide greater insight into the geodynamics of planetary differentiation. In eastern Australia, rapid Paleozoic–Mesozoic crustal growth was promoted by the oceanward retreat of a subduction-accretionary system following supercontinent assembly. This mechanism can reconcile the isotopic evidence for episodic crustal growth with the arc-like trace element budget of the continental crust, and may have played a greater role in rapid crust generation in the Precambrian than hitherto appreciated.

## Acknowledgements

Funded by NERC (NER/I/S/2000/00942) and ARC (DP0773029) fellowships to TK. Kevin Blake and Yi Hu assisted with the development of in situ Hf isotope techniques in the Advanced Analytical Centre at James Cook University. TK wishes to thank Richard Arculus for suggesting an isotopic study of crustal growth in eastern Australia. We are also grateful to Peter Cawood and Sasha Nemchin for provision of zircons from granitic units of the New England Orogen, to Ian Williams for supplying SHRIMP-dated zircons from intrusives of the Macquarie arc, and to David Foster and Drew Coleman for detailed comments on an earlier version of this manuscript. Two anonymous journal reviews greatly improved the manuscript in both clarity and scientific content and are much appreciated.

## Appendix A. Supplementary data

Supplementary data associated with this article can be found, in the online version, at doi:10.1016/j.epsl.2009.05.011.

## References

- Annen, C., Sparks, R.S.J., 2002. Effects of repetitive emplacement of basaltic intrusions on thermal evolution and melt generation in the crust. *Earth Planet. Sci. Lett.* 203, 937–955.
- Ansdell, K.M., Lucas, S.B., Connors, K., Stern, R.A., 1995. Kiseynew metasedimentary gneiss belt, Trans-Hudson orogen (Canada): back-arc origin and collisional inversion. *Geology* 23, 1039–1043.
- Belousova, E.A., Griffin, W.L., O'Reilly, S.Y., 2006. Zircon crystal morphology, trace element signatures and Hf isotope composition as a tool for petrogenetic modeling: examples from Eastern Australian granitoids. *J. Petrol.* 47, 329–353.
- Bolhar, R., Weaver, S.D., Whitehouse, M.J., Palin, J.M., Woodhead, J.D., Cole, J.W., 2008. Sources and evolution of arc magmas inferred from coupled O and Hf isotope systematics of plutonic zircons from the Cretaceous Separation Point Suite (New Zealand). *Earth Planet. Sci. Lett.* 268, 312–324.
- Bryant, C.J., Arculus, R.J., Chappell, B.W., 1997. Clarence River Supersuite: 250 Ma Cordilleran Tonalitic I-type intrusions in Eastern Australia. *J. Petrol.* 38, 975–1001.
- Bryant, C.J., Chappell, B.W., Bennett, V.C., McCulloch, M.T., 2004. Lithium isotope compositions of the New England Batholith: correlations with inferred source rock compositions. *Trans. R. Soc. Edinb. Earth Sci.* 95, 199–214.
- Cawood, P.A., 2005. Terra Australis Orogen: Rodinia breakup and development of the Pacific and Iapetus margins of Gondwana during the Neoproterozoic and Paleozoic. *Earth Sci. Rev.* 69, 249–279.
- Cawood, P.A., Buchan, C., 2007. Linking accretionary orogenesis with supercontinent assembly. *Earth Sci. Rev.* 82, 217–256.
- Chappell, B.W., White, A.J.R., Williams, I.S., 1991. A transverse section through granites of the Lachlan Fold Belt. Second Hutton Symposium Excursion Guide. Bureau of Mineral Resources, Geology and Geophysics.
- Clift, P., Vannuchi, P., 2004. Controls on tectonic accretion versus erosion in subduction zones: implications for the origin and recycling of the continental crust. *Rev. Geophys.* 42, 1–31.
- Coleman, D.S., Frost, T.P., Glazner, A.F., 1992. Evidence from the Lamarck Granodiorite for rapid Late Cretaceous crust formation in California. *Science* 258, 1924–1926.
- Collins, W.J., 1998. An evaluation of petrogenetic models for Lachlan Fold Belt granitoids: implications for crustal architecture and tectonic models. *Aust. J. Earth Sci.* 45, 483–500.
- Collins, W.J., 2002a. Hot orogens, tectonic switching and the creation of continental crust. *Geology* 30, 535–538.
- Collins, W.J., 2002b. The nature of extensional accretionary orogens. *Tectonics* 21, 1–12.
- Collins, W.J., Hobbs, B.E., 2001. What caused the Early Silurian change from mafic to silicic (S-type) magmatism in the eastern Lachlan Fold Belt. *Aust. J. Earth Sci.* 48, 25–41.
- Collins, W.J., Richards, S.W., 2008. Geodynamic significance of 'post-collisional' S-type granites in circum-Pacific orogens. *Geology* 36, 559–562.
- Collins, W.J., Wiebe, R.A., Healy, B., Richards, S.W., 2006. Replenishment, crystal accumulation and floor aggradation in the megacrystic Kameerka Suite, Australia. *J. Petrol.* 47, 2073–2104.
- Condie, K.C., 1998. Episodic continental growth and supercontinents: a mantle avalanche connection? *Earth Planet. Sci. Lett.* 163, 97–108.
- Crawford, A.J., Keays, R.R., 1987. Petrogenesis of Victorian Cambrian tholeiites and implications for the origin of associated boninites. *J. Petrol.* 28, 1075–1109.
- Crawford, A.J., Meffre, S., Squire, R.J., Barron, L.M., Fallon, T.J., 2007. Middle and Late Ordovician magmatic evolution of the Macquarie arc, Lachlan orogen, New South Wales. *Aust. J. Earth Sci.* 54, 181–215.
- Davidson, J.P., Arculus, R.J., 2006. The significance of Phanerozoic arc magmatism in generating continental crust. In: Brown, M., Rushmer, T. (Eds.), *Evolution and Differentiation of the Continental Crust*. Cambridge University Press, Cambridge, pp. 135–172.
- Draut, A.E., Clift, P.D., 2001. Geochemical evolution of arc magmatism during arc-continent collision, South Mayo, Ireland. *Geology* 29, 543–546.
- Fergusson, C.L., 2003. Ordovician–Silurian accretion tectonics of the Lachlan Fold Belt, southeastern Australia. *Aust. J. Earth Sci.* 50, 475–490.
- Fergusson, C.L., Fanning, C.M., 2002. Late Ordovician stratigraphy, zircon provenance and tectonics, Lachlan Fold Belt, southeastern Australia. *Aust. J. Earth Sci.* 49, 423–436.
- Foden, J.D., Elburg, M.A., Turner, S.P., Sandiford, M., O'Callaghan, J., Mitchell, S., 2002. Granite production in the Delamerian orogen, South Australia. *J. Geol. Soc. Lond.* 159, 557–575.
- Foden, J.D., Elburg, M.A., Dougherty-Page, J., Burt, A., 2006. The timing and duration of the Delamerian Orogeny: correlation with the Ross Orogen and implications for Gondwana assembly. *J. Geol.* 114, 189–210.
- Foster, D.A., Gray, D.R., 2000. The structure and evolution of the Lachlan Fold Belt (orogen) of Eastern Australia. *Annu. Rev. Earth Planet. Sci.* 28, 47–80.
- Foster, D.A., Gray, D.R., Spaggiari, C., 2005. Timing of subduction and exhumation along the Cambrian East Gondwana margin, and the formation of Paleozoic backarc basins. *GSA Bull.* 115, 105–116.
- Fu, B., Mernagh, T.P., Kita, N.T., Kemp, A.I.S., Valley, J.W., 2009. Distinguishing magmatic zircon from hydrothermal zircon: a case study from the Gidginbung high-sulphidation Au–Ag–(Cu) deposit, SE Australia. *Chem. Geol.* 259, 131–142.
- Gerdes, A., Worner, G., Finger, F., 2000. Hybrids, magma mixing and enriched mantle melts in post-collisional Variscan granitoids: the Rastenberg Pluton, Austria. *Geol. Soc. Lond. Spec. Publ.* 179, 415–431.
- Glen, R.A., 2005. The Tasmanides of eastern Australia. In: Vaughan, A.P.M., Leat, P.T., Pankhurst, R.J. (Eds.), *Terrane Processes at the Margins of Gondwana*. In: Special Publication, vol. 246. Geological Society, London, pp. 23–96.
- Glen, R.A., Korsch, R.J., Direen, N.J., Jones, L.E.A., Johnstone, D.W., Lawrie, K., Finlayson, D.M., Shaw, R.D., 2002. Crustal structure of the Ordovician Macquarie arc, eastern Lachlan Orogen, based on seismic-reflection profiling. *Aust. J. Earth Sci.* 49, 323–348.
- Gray, C.M., 1984. An isotopic mixing model for the origin of granitic rocks in southeastern Australia. *Earth Planet. Sci. Lett.* 70, 47–60.
- Gray, D.R., Foster, D.A., 2004. Tectonic evolution of the Lachlan Orogen, southeast Australia: historical review, data synthesis and modern perspectives. *Aust. J. Earth Sci.* 51, 773–818.
- Griffin, W.L., Wang, X., Jackson, S.E., Pearson, N.J., O'Reilly, S.Y., Xu, X., Zhou, X., 2002. Zircon chemistry and magma mixing, SE China: in-situ analysis of Hf isotopes, Tonglu and Pingtan igneous complexes. *Lithos* 61, 237–269.
- Healy, B., Collins, W.J., Richards, S.W., 2004. A hybrid origin for Lachlan S-type granites: the Murrumbidgee Batholith example. *Lithos* 78, 197–216.
- Hensel, H.D., McCulloch, M.T., Chappell, B.W., 1985. The New England Batholith: constraints on its derivation from Nd and Sr isotopic studies of granitoids and country rocks. *Geochim. Cosmochim. Acta* 49, 369–384.
- Hollings, P., Ansdell, K., 2002. Palaeoproterozoic arc magmatism imposed on an older backarc basin: implications for the tectonic evolution of the Trans-Hudson orogen, Canada. *GSA Bull.* 114, 153–168.
- Huang, M., Maas, R., Buick, I.S., Williams, I.S., 2003. Crustal response to continental collisions between Tibet, Indian, South China and North China Blocks: geochronological constraints from the Songpan–Garze orogenic Belt, western China. *J. Metamorph. Geol.* 21, 223–240.
- Hyndman, R.D., Currie, C.A., Mazzotti, S.P., 2005. Subduction zone back-arcs, mobile belts and orogenic heat. *GSA Today* 15, 4–10.
- Ireland, T.R., Flottmann, T., Fanning, C.M., Gibson, G.M., Preiss, W.V., 1998. Development of the early Paleozoic Pacific margin of Gondwana from detrital-zircon ages across the Delamerian Orogen. *Geology* 26, 243–246.
- Jahn, B.-M., Wu, F., Chen, B., 2000. Granitoids of the Central Asian Orogenic Belt and continental growth in the Phanerozoic. *Trans. R. Soc. Edinb. Earth Sci.* 91, 181–193.
- Keay, S., Collins, W.J., McCulloch, M.T., 1997. A three component Sr–Nd isotopic mixing model for granitoid genesis, Lachlan Fold Belt, eastern Australia. *Geology* 25, 307–310.
- Kemp, A.I.S., 2003. Plutonic boninite-like rocks in an anatectic setting, and their tectonic implications for the Delamerian Orogen in southeast Australia. *Geology* 31, 371–374.
- Kemp, A.I.S., Gray, C.M., Anderson, J.A.C., Ferguson, D.J., 2002. The Delamerian Glenelg tectonic zone, western Victoria: characterization and synthesis of igneous rocks. *Aust. J. Earth Sci.* 49, 201–224.
- Kemp, A.I.S., Wormald, R.J., Whitehouse, M.J., Price, R.C., 2005. Hf isotopes in zircon reveal contrasting sources and crystallisation histories for alkaline to peralkaline granites of Temora, southeastern Australia. *Geology* 33, 797–800.
- Kemp, A.I.S., Hawkesworth, C.J., Paterson, B.A., Kinny, P., 2006. Episodic growth of the Gondwana Supercontinent from hafnium and oxygen isotopes in zircon. *Nature* 439, 580–583.
- Kemp, A.I.S., Hawkesworth, C.J., Foster, G.L., Paterson, B.A., Woodhead, J.D., Hergt, J.M., Gray, C.M., Whitehouse, M., 2007. Magmatic and crustal differentiation history of granitic rocks from Hf–O isotopes in zircon. *Science* 315, 980–983.
- Kemp, A.I.S., Hawkesworth, C.J., Paterson, B.A., Foster, G.L., Kinny, P.D., Whitehouse, M.J., Maas, T., EIMF, 2008. Exploring the plutonic–volcanic link: a zircon U–Pb, Lu–Hf and O isotope study of paired volcanic and granitic units from southeastern Australia. *Trans. R. Soc. Edinb. Earth Sci.* 97, 337–355.
- King, P.L., White, A.J.R., Chappell, B.W., 1997. Characterization and origin of aluminous A-type granites of the Lachlan Fold Belt, southeastern Australia. *J. Petrol.* 36, 371–391.
- Lackey, J.S., Valley, J.W., Saleeby, J.B., 2005. Supracrustal input to magmas in the deep crust of Sierra Nevada batholith: evidence from high  $\delta^{18}\text{O}$  zircon. *Earth Planet. Sci. Lett.* 235, 315–330.
- Landenberger, B., Collins, W.J., 1996. Derivation of A-type granites from a dehydrated charnockitic lower crust: evidence from the Chaelundi Complex, Eastern Australia. *J. Petrol.* 37, 145–170.
- Landenberger, B., Farrell, T.R., Offler, R., Collins, W.J., Whitford, D.J., 1995. Tectonic implications of Rb–Sr biotite ages of the Hillgrove Plutonic Suite, New England Fold Belt, N.S.W., Australia. *Precambrian Res.* 71, 251–263.
- Maas, R., Nicholls, I.A., Legg, C., 1997. Igneous and metamorphic enclaves in the S-type Deddick Granodiorite, Lachlan Fold Belt, SE Australia: petrographic, geochemical and Nd–Sr isotopic evidence for crustal melting and magma mixing. *J. Petrol.* 38, 815–841.
- McCulloch, M.T., Bennett, V.C., 1994. Progressive growth of the Earth's continental crust and depleted mantle: geochemical constraints. *Geochim. Cosmochim. Acta* 58, 4717–4738.
- McCulloch, M.T., Chappell, B.W., 1982. Nd isotopic characteristics of S- and I-type granites. *Earth Planet. Sci. Lett.* 58, 51–64.
- Murphy, J.B., Nance, R.D., 2002. Sm–Nd isotopic systematics as tectonic tracers: an example from West Avalonia in the Canadian Appalachians. *Earth Sci. Rev.* 59, 77–100.
- Myers, J.S., Shaw, R.D., Tyler, I.M., 1996. Tectonic evolution of Proterozoic Australia. *Tectonics* 15, 1431–1446.
- O'Neil, J.R., Shaw, S.E., Flood, R.H., 1977. Oxygen and hydrogen isotope compositions as indicators of granite genesis in the New England Batholith, Australia. *Contrib. Mineral. Petrol.* 62, 313–328.
- Parman, S.W., 2007. He isotopic evidence for episodic mantle melting and crustal growth. *Nature* 446, 900–903.
- Patchett, P.J., Chase, C.G., 2002. Role of transform continental margins in major crustal growth episodes. *Geology* 30, 39–42.
- Pearson, D.G., Parman, S.W., Nowell, G.M., 2007. A link between large mantle melting events and continent growth seen in osmium isotopes. *Nature* 449, 202–205.
- Plank, T., 2005. Constraints from thorium/lanthanum on sediment recycling at subduction zones and the evolution of continents. *J. Petrol.* 46, 921–944.
- Samson, S.D., McClelland, W.D., Patchett, P.J., Gehrels, G.E., Anderson, R.G., 1989. Evidence from Nd isotopes for mantle contributions to Phanerozoic crustal genesis in the Canadian Cordillera. *Nature* 337, 705–709.

- Schmitz, M.D., Vervoort, J.D., Bowring, S.A., Patchett, P.J., 2004. Decoupling of the Sm–Nd and Lu–Hf isotope systems during the evolution of granulitic lower crust beneath southern Africa. *Geology* 32, 405–408.
- Sengor, A.M.C., Natal'in, B.A., Burtman, V.S., 1993. Evolution of the Altaid tectonic collage and Palaeozoic crustal growth in Eurasia. *Nature* 364, 299–307.
- Stein, M., Hofmann, A.W., 1994. Mantle plumes and episodic crustal growth. *Nature* 372, 63–68.
- Taylor, S.R., 1967. The origin and growth of continents. *Tectonophysics* 4, 17–34.
- Tiepolo, M., Tribuzio, R., 2008. Petrology and U–Pb geochronology of amphibole-rich cumulates of sanukitic affinity from Husky Ridge (Northern Victoria Land, Antarctica): insights into the role of amphibole in the petrogenesis of subduction-related magmas. *J. Petrol.* 49, 937–970.
- Turner, S.P., 1996. Petrogenesis of late-Delamerian gabbroic complex at Black Hill, South Australia: implications for convective thinning of the lithospheric mantle. *Mineral. Petrol.* 56, 51–89.
- Turner, S.P., Foden, J.D., Morrison, R.S., 1992. Derivation of some A-type magmas by fractionation of basaltic magma: an example from the Padthaway Ridge, South Australia. *Lithos* 28, 51–179.
- Turner, S.P., Adams, C.J., Flottmann, T., Foden, J.D., 1993. Geochemical and geochronological constraints on the Glenelg River Complex, western Victoria. *Aust. J. Earth Sci.* 40, 275–292.
- Valley, J.W., 2003. Oxygen isotopes in zircon. *Rev. Mineral. Geochem.* 53, 343–380.
- Vervoort, J.D., Patchett, P.J., Blichert-Toft, J., Albarede, F., 1999. Relationships between Lu–Hf and Sm–Nd isotopic systems in the global sedimentary system. *Earth Planet. Sci. Lett.* 168, 79–99.
- Waight, T.M., Maas, R., Nicholls, I.A., 2001. Geochemical investigations of microgranitoid enclaves in the S-type Cowra Granodiorite, Lachlan Fold Belt, SE Australia. *Lithos* 56, 165–186.
- White, A.J.R., Chappell, B.W., 1977. Ultrametamorphism and granitoid genesis. *Tectonophysics* 43, 7–22.
- Wormald, R.J., Price, R.C., Kemp, A.I.S., 2004. Geochemistry and Rb–Sr geochronology of the alkaline–peralkaline Narraburra Complex, central southern New South Wales. *Aust. J. Earth Sci.* 51, 369–384.
- Yang, J.-H., Wu, F.-Y., Wilde, S.A., Xie, L.-W., Yang, Y.-H., Liu, X.-M., 2007. Tracing magma mixing in granite genesis: *in situ* U–Pb dating and Hf-isotope analysis of zircons. *Contrib. Mineral. Petrol.* 153, 177–190.
- Zandt, G., Gilbert, H., Owens, T.J., Ducea, M., Saleeby, J., Jones, C.H., 2004. Active foundering of a continental arc root beneath the southern Sierra Nevada in California. *Nature* 431, 41–46.